Interdependence of ICD rates in paired quantum dots on geometry

Fabian Weber[*], Emad F. Aziz[†‡§], Annika Bande [¶]

April 12, 2017

Abstract

Using state-of-the-art antisymmetrized multiconfiguration time-dependent Hartree (MCTDH) electron dynamics calculations we study the interdependence of the intermolecular Coulombic decay (ICD) process on the geometric parameters of a doubly-charged paired quantum dot (PQD) model system in the framework of the effective mass approximation (EMA).

We find that ICD displays a maximum rate for a certain geometry of the electron-emitting quantum dot, which is simultaneously dependent on both the distance between the quantum dots as well as the photon-absorbing quantum dot's geometry. The rate maximum is shown to be caused by the competing effects of polarization of electron density and Coulomb repulsion.

The ICD rate-maximized PQD geometry in GaAs QDs yields a decay time of 102.39 ps. It is given by two vertically-aligned cylindrical QDs with radii of 14.42 nm separated by 86.62 nm. The photon absorbing QD then has a height of 46.59 nm and the electron emitting QD a height of 16.33 nm.

April 12, 2017

Keywords: intermolecular Coulombic decay, electron dynamics, quantum dots, quantum size effect, geometric control ■

[*]Institute of Methods for Material Development, Helmholtz-Zentrum Berlin für Materialien und Energie GmbH, Albert-Einstein-Str. 15, 12489 Berlin, Germany

[†]Institute of Methods for Material Development, Helmholtz-Zentrum Berlin für Materialien und Energie GmbH, Albert-Einstein-Str. 15, 12489 Berlin, Germany

[‡]Department of Physics, Freie Universitt Berlin, Arnimallee 14, 14195 Berlin, Germany

[§]School of Chemistry, Monash University, Clayton 3800, VIC, Australia

[¶]Institute of Methods for Material Development, Helmholtz-Zentrum Berlin für Materialien und Energie GmbH, Albert-Einstein-Str. 15, 12489 Berlin, Germany

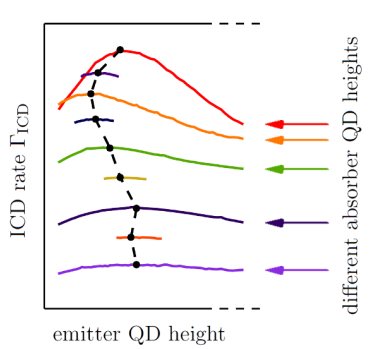

Using electron dynamics calculations, the intermolecular Coulombic decay (ICD) rate in a paired quantum dot (PQD) model system is optimized by a multidimensional scan of geometric parameters. An ICD rate-limiting maximum is found that is non-trivially interdependent on all geometric parameters. The reason for the occurence of the maxima is identified as the competing effects between Coulomb repulsion and electronic polarization, which expands the understanding of the ICD process in QDs.

INTRODUCTION

The intermolecular Coulombic decay (ICD)[1] process presents an indirect pathway for using the energy of a photon to eject a bound electron. It is based on a photo-induced auto-ionization process where, in contrast to the Auger decay[2], the auto-ionized electron is emitted from a different molecule than the initially excited one. The reason for this behaviour is directly related to the energetic regime of the ICD process and the electronic structure. While Auger processes are initiated using highly-energetic radiation (i.e. exciting core-shell electrons), the ICD process is initiated in a rather low-energy regime[1]. For such low excitation energies, the resonance state leading to the decay is not high enough in energy to undergo a direct ionization process on the same excited species. It may, however, decay to a state where the ionization took place on a different species via electron correlation[3].

Over the last two decades since its postulation, many different molecular clusters have been shown both experimentally[4–6] as well as theoretically[7–9] to undergo ICD. In all studies, the efficiency of the process was proven to be heavily dependent on the electronic structure of the respective molecular clusters. The ICD rate Γ_{ICD} is often described in terms of a virtual photon transfer process in an asymptotic approximation[10]

$$\Gamma_{\mathrm{ICD}} = \frac{3}{4\pi} \frac{\tilde{\sigma}_{\mathrm{E}}(E_{\mathrm{vph}}) \cdot \tau_{\mathrm{A}}^{-1}}{R^6 \cdot E_{\mathrm{vph}}^4}, \tag{1}$$

which assumes that the excited and the emitted electron are not interacting with each other and that their separate wavefunctions do not overlap. In the above expression $\tilde{\sigma}_{\mathrm{E}}(E_{\mathrm{vph}})$ is the photonionization cross section of the electron-emitting species at energy E_{vph}, τ_{A}^{-1} is the inverse life time corresponding to a spontaneous radiative decay of the photon-absorbing species' excited initial state and E_{vph} is the virtual photon energy released upon relaxation of this state. As all the quantities are heavily dependent on the electronic structure, the released electrons have very characteristic kinetic energy profiles[11].

In contrast to molecules, the electronic structure of quantum dots (QDs) may be tailor made[12] to a very high degree. Consequently they are promising candidates for utilizing the ICD process in different energetic regimes and for various purposes. To study electron dynamics in such extended systems, we combine the effective mass approximation

(EMA)[13] with the antisymmetrized variant of the multiconfiguration time-dependent Hartree (MCTDH) method as implemented in the Heidelberg MCTDH software distribution[14,15]. Due to the quantum confinement of the electrons in nanoscopic materials[16], one may limit the calculation to only the two electrons directly involved in the ICD process, which are then confined in a model potential that mimics the shape of the nanoscopic particle.

Using this approach, we were able to formulate a paired quantum dot (PQD) model system that undergoes ICD[17]. The system is comprised of one designated photon-absorbing QD (AQD) and one electron-emitting QD (EQD). We conducted different studies on the interaction of the PQD with laser fields[18,19], as well as on the effects of geometrical changes on the ICD rate and electronic structure. For instance, we were able to reproduce the R^{-6} behaviour of the ICD rate as given in the asymptotic approximation for inter-QD distances with vanishing orbital overlap[17].

In our most recent study on the geometric set-up, the height of the AQD as well as the width of both QDs were varied separately[20]. From the variation of the AQD height, we concluded that the ICD rate is strongly interdependent on both QDs simultaneously, as we found a non-trivial behaviour different from $\Gamma \approx E_{\mathrm{vph}}^{-4}$ as given in the asymptotic approximation (eq. (1)). Also, we could show that the QD width variation had an impact on the ICD rate Γ_{ICD}, although the widths have no obvious connection to the asymptotic approximation. The geometric set-up which resulted in the fastest ICD rate found in that study was a pair of vertically aligned cigar-shaped QDs.

Owing to the possibility to factorize the three-dimensional problem into a truly one-dimensional one and the large speed-up achieved[20], it is now possible to not only study how changes in the remaining unprobed EQD height parameter affect the ICD rate Γ_{ICD}, but also to address the interdependence of Γ_{ICD} on changes in several geometric parameters simultaneously. Based on the understanding of the interplay of these parameters, we may then formulate optimal geometries for desired experimental observables. In this work we search for a geometry that could be applied in an ultrafast and efficient photon detection device by optimizing the decay rate. When the ICD rate is maximized, other processes that could quench the signal in such detection devices like phononic dissipation of the photon energy are less likely to occur. Additionally, the approach also allows to draw conclusions

about the physical limitations of the ICD process in charged QDs.

This paper is organized as follows. In the theory section we will outline the general equations describing the paired QD system and explain the procedure used to calculate the ICD rates for a rigorous scan of over 1000 different geometries. The results section first summarizes shortly the geometric control of the ICD rate through the AQD height and inter-QD distance known from preceding studies[17,20] and thereafter focuses on the effects on Γ_{ICD} upon varying the EQD geometry, as we did not cover this parameter yet. After that we investigate how the ICD rate depends on several geometric PQD parameters simultaneously and especially whether there are trends in the interdependence as well as limitations of the ICD rate to be found. Finally, we conclude our results and discuss how to predict a geometry with a maximized ICD rate.

THEORY

Paired quantum dot model

The one-dimensional paired quantum dot (PQD) model system is given by two differently-shaped inverse Gaussian potentials in z direction

$$V_{\mathrm{PQD}}(z_i) \;=\; \begin{cases} \underbrace{-D_{\mathrm{A}}\; e^{-b_{\mathrm{A}}(z_i+\frac{R}{2})^2}}_{V_{\mathrm{A}}}\;\underbrace{-D_{\mathrm{E}}\; e^{-b_{\mathrm{E}}(z_i-\frac{R}{2})^2}}_{V_{\mathrm{E}}}, & \text{if} \quad z_i \in [-L_z,\ldots,L_z] \\ \infty, & \text{otherwise.} \end{cases} \tag{2}$$

For calculation purposes, the PQD is placed inside a relatively broad infinite potential well with box length $2L_z$. In this expression, the indices A and E stand for the photon absorbing QD (AQD) and electron emitting QD (EQD), respectively. The depth parameter $D_{\mathrm{A/E}}$ encodes information on the material composition while $b_{\mathrm{A/E}}$ and R are geometrical parameters. The inter-QD distance R gives the distance between the inverse Gaussian potential minima and the QD height $h_{\mathrm{A/E}}$ is connected to $b_{\mathrm{A/E}}$ through the full width at half minimum value of the inverse Gaussian $h_{\mathrm{A/E}} = 2\sqrt{(\ln(2)/b_{\mathrm{A/E}})}$. Note that the effective distance $R_{\mathrm{eff}} = R - \frac{h_{\mathrm{A}}+h_{\mathrm{E}}}{2}$ which is a measure for the distance between the QD interfaces is

affected by changes in the individual QD heights.

To offer a more concrete description, the parameter values which enter the calculations in atomic units (indexed a.u.) were translated to material specific real units (indexed EMA) by using the effective mass approximation (EMA). Throughout the study we convert into units of GaAs with the effective mass for the electron of $m_{\mathrm{e}}^{*} = 0.063\ m_{\mathrm{e}}$ and the dielectric constant $\kappa_{\mathrm{GaAs}} = 12.9$:[21]

$$R^{\mathrm{EMA}} = R_{\mathrm{a.u.}}\ \frac{\kappa m_{\mathrm{e}}}{m_{\mathrm{e}}^{*}}\ a_0, \quad E^{\mathrm{EMA}} = E_{\mathrm{a.u.}}\frac{\kappa^2 m_{\mathrm{e}}}{m_{\mathrm{e}}^{*}}\ E_{\mathrm{h}}, \quad t^{\mathrm{EMA}} = t_{\mathrm{a.u.}}\ \frac{\hbar}{E^{\mathrm{EMA}}}. \tag{3}$$

In this study we vary predominantly the parameter b_{E}. Additionally, simultaneous variation of the parameters b_{A} and R serves to probe the interdependence of the ICD rate on all parameters for the first time. In all cases, the PQD potential parameters are chosen such, that there is exactly one one-electron level in the EQD and two one-electron levels in the AQD. The parameter ranges may be taken from table 1 in real units of GaAs and in atomic units. Note that we conducted one large scan of $h_{\mathrm{E}} \in [11.41, \ldots, 23.29]$ nm for one specific pair of default values $h_{\mathrm{A}} = 18.04$ nm and $R = 86.62$ nm that were used in our other studies[17,19,20,23]. For any other combination of h_{A} and R we diminished the interval to $h_{\mathrm{E}} = [14.73, \ldots, 19.34]$ nm. The box length was chosen as $L_z = 65.0$ a.u. (which translates to 704.31 nm). Figure 1 visualizes the PQD shapes for the extreme values for both QD heights and inter-QD distances R.

The Hamiltonian for the one-dimensional two-electron system in atomic units ($m_e = 1$ a.u., $\hbar = 1$ a.u., $\frac{1}{4\pi\epsilon_0} = 1$ a.u.) is given by

$$\hat{H}_{\mathrm{PQD}}(z_1, z_2) = \sum_{i=1}^{2}\Big(-\frac{1}{2}\Big(\frac{\partial}{\partial z_i}\Big)^2 + V_{\mathrm{PQD}}(z_i)\Big) + V(|z_1 - z_2|)_{\mathrm{1D}}^{(\omega_\perp)} \tag{4}$$

with $V(|z_1 - z_2|)_{\mathrm{1D}}^{(\omega_\perp)}$ being a pseudo one-dimensional Coulomb interaction potential of the form[22]

$$V(|z_1 - z_2|)_{\mathrm{1D}}^{(\omega_\perp)} = \sqrt{\frac{\pi}{2l^2}}\ e^{\xi^2}\Big(1 - \mathrm{erf}(\xi)\Big). \tag{5}$$

The potential assumes the electrons to be confined in a harmonic oscillator potential perpendicular to z with strength $\omega_\perp$. The quantity ξ is given as

$$\xi(|z_1 - z_2|) = \Big(\sqrt{\frac{1}{2l}}\,|z_1 - z_2|\Big), \tag{6}$$

with $l = \sqrt{1/\omega_\perp}$ in atomic units. The widths of both QDs in the pseudo one-dimensional description was fixed to 28.84 nm by choosing $\omega_\perp = 1.0$ a.u., which is the same value as used in previous studies[17]. There, we also presented a proof of principle, by showing that the pseudo one-dimensional calculation suffices to reproduce the results of a full three-dimensional calculation.

Solving the time-independent Schrödinger equation with $\hat{H}_{\mathrm{PQD}}$ of eq. (4) yields a set of different eigenstates with different physical meaning. Eigenstates which show electron density confined in either of the QDs while not having any energetically lower-lying eigenstate that would show electron density outside either of the QDs shall be termed bound eigenstates. We shall refer to eigenstates that display electron density of at least one electron outside of the QDs as continuum-*like*, although they are technically still bound inside the simulation box and as such, cannot describe a real continuum. Eigenstates which lie higher in energy than the first continuum-like eigenstate but show pronounced electron density mainly inside the QDs again will then be referred to as resonance-like states.

Electron dynamics calculations

As explained before, the ICD process starts from a resonance state, where the AQD electron is in its first excited state while the EQD electron remains in its ground state. For easier notation we shall call this resonance state A1E0 and the overall ground state A0E0. Both of them may be approximated by eigenstates of the system Hamiltonian eq. (4). The resonance-like A1E0 eigenstate obtained from this Hamiltonian is then used as the initial state for the propagation of the electronic wavepacket applying the non-Hermitian propagation Hamiltonian

$$\hat{H}_{\mathrm{prop}}(z_1, z_2) = \sum_{i=1}^{2}\left(V_{\mathrm{PQD}}(z_i) - \frac{1}{2}\Big(\frac{\partial}{\partial z_i}\Big)^2 - iW_{\mathrm{L}}(z_i) - iW_{\mathrm{R}}(z_i)\right) + V(|z_1 - z_2|)_{\mathrm{1D}}^{(\omega_\perp)}. \tag{7}$$

In solving the time-dependent Schrödinger equation, the real A1E0 resonance state is obtained from the initial resonance-like A1E0 state after the first few propagation steps,

and then decays exponentially. The propagation Hamiltonian eq. (7) contains additional complex absorbing potentials (CAP)[24]

$$W_{\mathrm{L,R}}(z_i) = \eta_{\mathrm{L,R}}(z_i - z_{\mathrm{L,R}})^n \Theta(z_i - z_{\mathrm{L,R}}) \tag{8}$$

at the left (L) and right (R) side of the paired QD. In this expression, the Heaviside function $\Theta(z_i - z_{\mathrm{L,R}})$ ensures that the potentials only act beyond the onset points $z_{\mathrm{L,R}}$. Onsets and CAP order n were fixed to be $z_{\mathrm{L,R}} = \pm 325$ nm and $n = 4$, respectively. $\eta_{\mathrm{L,R}}$ are the CAP strength parameters that were equal on both sides. They were adjusted for each calculation separately to minimize reflections of the continuum electron with a defined E_{kin} at the quantum well boundaries.

The improved block relaxation[15] utilizing the system Hamiltonian of eq. (4) as well as the propagation of the wavepacket in real time are performed within a multiconfiguration time-dependent Hartree (MCTDH) ansatz. Here we utilize a wavefunction of the form

$$\Psi(z_1, z_2, t) = \sum_{j_1=1}^{n_1} \sum_{j_2=1}^{n_2} A_{j_1 j_2}(t) \varphi_{j_1}^{(1)}(z_1, t) \varphi_{j_2}^{(2)}(z_2, t), \tag{9}$$

where each degree of freedom z_i is represented by n_i orthonormal and time-dependent single particle functions (SPF) φ_{j_i}. Every set of indices $j_1 j_2$ is connected to a specific product of SPFs and represents one configuration in the complete configuration space. Finally, each of the configurations is weighted by a time-dependent factor $A_{j_1 j_2}(t)$. We are treating a system of triplet spin electrons by antisymmetrizing the weights according to $A_{ji} = -A_{ij}$[17,19].

We choose 48 SPFs for each of the electrons' z coordinates for the improved relaxation calculation with the system Hamiltonian eq. (4). For the propagation of the resonance state in real time with the propagation Hamiltionan eq. (7), the A1E0 wavepacket is expressed using a reduced number of 12 SPFs. The SPFs were expanded in terms of a discrete variable representation (DVR)[15] into a set of 182 orthogonal sine DVR functions on a grid inside the quantum well boundaries. The grid resolution (0.129 grid points per nm) as well as the integrator accuracy for the time-propagation were adopted from earlier calculation-speed optimized scans[20]. Convergence of the ICD rates with respect to variations in the box length and grid resolution was thoroughly checked for variations of the parameters of the

PQD geometry.

The solution of the time-dependent Schrödinger equation starting from the resonance-like A1E0 Φ_{A1E0} wavepacket using the propagation Hamiltonian eq. (7) yields a decaying wavepacket $\Psi^{Decay}_{\mathrm{A1E0}}(z_1, z_2, t)$ whose norm $N(t) = \sqrt{\int\int \Psi(z_1, z_2, t)^* \Psi(z_1, z_2, t) dz_1 dz_2}$ decreases over time when electron density leaks into the continuum, i.e. into the CAPs. The ICD rate Γ_{ICD} can be obtained from the exponential decay of the squared autocorrelation function

$$|a(t)|^2 = |\langle\ \Phi_{\mathrm{A1E0}}(z_1, z_2, t = 0)\ |\ \Psi^{Decay}_{\mathrm{A1E0}}(z_1, z_2, t)\ \rangle|^2 \propto e^{-\Gamma_{\mathrm{ICD}} t}. \tag{10}$$

RESULTS AND DISCUSSION

State-of-the-art geometric control in PQDs

In our first work on the geometric control of ICD in PQDs[17] we focused on changes in the inter-QD distance R and whether it was possible to reproduce the R^{-6} behaviour for the ICD rate Γ_{ICD} as suggested from the asymptotic approximation eq. (1). While for intermediate and long inter-QD distances the $\Gamma_{\mathrm{ICD}} \approx R^{-6}$ was obtained, very low inter-QD distances lead to a big enhancement of the ICD rates. This effect was attributed to the overlap of the QD potential wells alongside the A1 and E0 one-electron orbitals - which is a known limitation of the asymptotic approximation.[10]

The second study on geometric control[20] was then focused on changing the AQD height h_{A} as well as the width of both QDs. It was shown that changes in h_{A} heavily influence both the virtual photon energy as well as the Coulomb interaction. Low values of h_{A} resulted in higher virtual photon energies E_{vph} as the quantum confinement in smaller QDs separates the eigenstates more and more. It was not possible though, to reproduce the E^{-4}_{vph} behaviour of the ICD rate, as changes in the AQD height have a seemingly much more complex impact on the asymptotic approximation. For example, low AQD heights lead both to a smaller Coulomb interaction due to the lower effective distance $R_{\mathrm{eff}} = R - \frac{h_{\mathrm{A}} + h_{\mathrm{E}}}{2}$ between the two electrons, as well as a change of the photoionization cross section $\tilde{\sigma}_{\mathrm{E}}(E_{\mathrm{vph}})$ through the change in E_{vph}. However, all findings showed that lower AQD heights always lead to lower

ICD rates.

Finally, to give an idea about the sensitivity of the ICD rate on these parameters, we fix every other parameter to the default case (i.e. $h_{\mathrm{E}} = 18.04$ nm, $h_{\mathrm{A}} = 36.08$ nm and $R = 86.62$ nm). When then changing h_{A} from 47 nm to 29 nm a moderate increase of the decay time from 116 ps to 434 ps is obtained. If, however, R is changed from 87 nm to 173 nm the decay times increase significantly from 236 ps to 18 ns.

Variation of the EQD height

Static Properties

To understand the general characteristics when changing the EQD geometry, we started investigating the electronic structure and other static properties of the resonance state. To achieve this, we first performed improved block relaxation calculations using the system Hamiltonian (eq. (4)) at a fixed, default inter-QD distance $R = 86.62$ nm and AQD height of $h_{\mathrm{A}} = 36.08$ nm. Figure 2 shows the one-electron densities $|\Phi(z_1)|^2 = \int \Phi^*(z_1, z_2)\Phi(z_1, z_2)dz_2$ of the most important electronic eigenstates, namely the resonance-like state A1E0 and ground state A0E0 of which the eigenvectors were taken for further analysis. One can see that both the A0E0 and the A1E0 states represent cases, where the electrons are localized inside the QDs as the density is close to zero outside the QDs.In addition to these states, the first continuum-like eigenstate's electron density is shown. Here, one electron is in the ground state of the AQD while the other electron is outside either QD. For easier notation, we will call such states to be of A0C type.

Figure 3 depicts the eigenenergies E_{A1E0} and E_{A0E0} and the continuum-like states' eigenenergies for the large scan of h_{E}. For the sake of better readability, only every second of the continuum-like states is included in the figure. The eigenenergies were shifted such, that the first continuum-like eigenstate has an energy of zero.

The ground state and resonance-like state energies are both lowering for higher h_{E}. As both states have one electron in the E0 state, their eigenenergies are affected by the same magnitude and in the same way as we observe for the one-electron E0 state eigenenergies. This goes along with the fact that for higher h_{E} the EQD electron's movement is less and

less restricted due to the widening of the potential well.

Furthermore, it can be seen that the energies of the low-lying continuum-like states stay almost constant. This is due to the fact that they are of A0C type for most geometries, which means that they have no electron density inside the EQD region, and therefore are not affected by changes of h_{E}. The energetically highest states shown are CE0 continuum-like states. Here the AQD electron is in the continuum while the EQD has one electron in its only bound state. Continuum-like states of this type follow the exact same energetic decrease as the A0E0 and A1E0 states.

As the energy of the A1E0 state decreases for increasing h_{E} while the A0C type states stay constant in energy, at some points the states must cross each other. The state A1E0 which we declare as the j^{th} state at some h_{E} turns into one of A0C type when going towards higher h_{E}. The A1E0 state is then represented by the $(j-1)^{\mathrm{th}}$ state. A closer look (cf. Fig. 4) reveals an avoided crossing with a wide energy gap at every second of these transitions. Here the states become almost degenerate (cf. Fig. 5) over a large range of h_{E}, while every other transition (which we refer to as non-degenerate) is less affected. The former crossings are with those A0C states that have continuum contributions to the right side, the latter to the left.

Another important quantity that is directly related to the ICD process is the expectation value of the Coulomb repulsion $E_{\mathrm{Cou}} = \langle\Phi|\frac{1}{r_{12}}|\Phi\rangle$ of the real resonance state. Unfortunately, the expectation value obtained from the resonance-like state may differ significantly from the real one, because the fromer is heavily influenced by the admixture of continuum-like contributions to the real A1E0 state's wavefunction near the avoided crossings. We thus decided to approximate the expectation value by utilizing a shortly propagated wavepacket $\tilde{\Phi}^{prop}_{\mathrm{A1E0}}$ that was obtained by applying the non-Hermitian propagation Hamiltonian (eq. (7)) for the propagation of the resonance-like eigenstate of Hamiltonian eq. (4). This way, the degeneracy caused by the continuum contributions of the wavefunction would be remedied in the first few time steps by the CAP, which absorbs all continuum-like state's electron density. As the norm of this wavepacket is different from unity, the final expression for the approximation is

$$\tilde{E}_{\mathrm{Cou}} = \left| \frac{\langle \tilde{\Phi}^{prop}_{\mathrm{A1E0}} | \frac{1}{z_{12}} | \tilde{\Phi}^{prop}_{\mathrm{A1E0}} \rangle}{\langle \tilde{\Phi}^{prop}_{\mathrm{A1E0}} | \tilde{\Phi}^{prop}_{\mathrm{A1E0}} \rangle} \right| \qquad \text{with} \qquad z_{12} = |z_1 - z_2| \tag{11}$$

Figure 6 depicts $\tilde{E}_{\mathrm{Cou}}$ for different values of h_{E}. The Coulomb repulsion obtained by the remedied wavefunction still shows pronounced spikes that can be clearly assigned to values of h_{E} near the avoided crossings. One can see that for increasing EQD height, $\tilde{E}_{\mathrm{Cou}}$ decreases slightly with a local minimum at $h_{\mathrm{E}} = 18.91$ nm. Note that the value of the inverse of $\tilde{E}_{\mathrm{Cou}}$ conveniently corresponds to a mean inter-electron distance $\bar{r}_{12}$ in the two-electron system. Using the highest and lowest values of $\tilde{E}_{\mathrm{Cou}}$ (i.e. 1.294 and 1.281 meV, respectively), we can see that all values in $\bar{r}_{12}$ lie within a range of 86.29 to 87.14 nm, which is in close vicinity to the actual inter-QD distance $R = 86.62$ nm. The reason for the overall trend in $\tilde{E}_{\mathrm{Cou}}$ can be connected to the fact that for a broader EQD potential well the E0 electron may move a bit farther away from the A1 electron, which minimizes the Coulomb repulsion and polarizes the E0 electron density slightly away from the AQD, i.e. to the right side. As a competitive effect, the undistorted E0 state gets stabilized when going towards higher values of h_{E}, such that at some point the polarization of the EQD electron density presents less of an energetic gain than assuming the undistorted density.

To reinforce the above statement, we calculate a measure for the polarization of the wavepacket as the expectation value of the total dipole moment from the shortly-propagated wavepacket as

$$\langle q \rangle = \frac{\langle \tilde{\Phi}^{prop}_{\mathrm{A1E0}} | \sum_{i=1}^{2} z_i | \tilde{\Phi}^{prop}_{\mathrm{A1E0}} \rangle}{\langle \tilde{\Phi}^{prop}_{\mathrm{A1E0}} | \tilde{\Phi}^{prop}_{\mathrm{A1E0}} \rangle} \tag{12}$$

As the potential wells are centered around $z = 0$, expression (12) is giving information on whether the electrons are more located to the right (positive sign, i.e. side of the EQD) or left (negative sign, side of the AQD). As can be seen from figure 7 the electron density of the two-electron wavepacket is indeed moving to the right for increasing h_{E}, as $\langle q \rangle$ increases. The spikes in the curve are again related to the near-degenerate A1E0 states.

Electron Dynamics

To analyse the dynamics of the ICD process, the A1E0 resonance-like states obtained as eigenstates of Hamiltonian eq. (4) for the different geometries were chosen as initial wavepackets and each was propagated in time for 320 ps (converted to time of the GaAs QDs from 5000 a.u.) using the non-Hermitian propagation Hamiltonian $\hat{H}_{\text{prop}}(z_1, z_2)$ (eq. (7)). The numerical time-propagation steps were adapted dynamically by the program to ensure time-reversibility of the wavepacket's trajectory[14]. On average, the propagation step size was about 90 fs. After the propagation, the squared autocorrelation function $|a(t)|^2$ (eq. (10)) was evaluated and the ICD rate Γ_{ICD} extracted. In table 2 we list a selection of representative examples. The respective autocorrelation plots are shown in figure 8.

The geometries shown here are derived from the default parameters $h_{\text{A}} = 36.08$ nm, $h_{\text{E}} = 18.04$ nm, and $R = 86.62$ nm (denoted "0" in the legend), from which we then alter the EQD height to both lower as well as higher values. Note that the number in front of the minus/plus indicates roughly how many nm smaller/larger the respective EQD height is. As one can see, there seems to be no monotonous trend in the ICD rate Γ_{ICD} with respect to h_{E}, because we find lower decay rates for both higher, as well as lower EQD heights. Hence, we expect at least one local maximum within the screened parameter range. To prove this, we plot the decay rates Γ_{ICD} for fixed $R = 86.62$ nm and $h_{\text{A}} = 36.08$ nm against a large scan of the EQD height h_{E} (cf. Fig. 9).

One can see that there is indeed a single maximum in the ICD rate Γ_{ICD} at an EQD height of about $h_{\text{E}} = 16.01$ nm. While for increasing EQD heights there is a slow decline in Γ_{ICD}, towards lower h_{E} the ICD rate decreases very fast. The reason for this behaviour can be explained when considering the aforementioned competing effect of the polarization[25] versus the Coulomb repulsion, which was discussed for the same parameter set in the previous section.

For low h_{E} the polarization $\langle q \rangle$ is increasing rapidly (cf. Fig. 7), whereas $\tilde{E}_{\text{Cou}}$ is decreasing rather slowly. As the Coulomb repulsion is thus still high for low h_{E}, the stronger and stronger polarization of the electron density towards the EQD facilitates the ICD process, as the overall electron density is shifted towards the QD from which they may leave the

system. However, as the electron density inside the EQD shifts farther away from the AQD upon further increasing h_{E}, the Coulomb repulsion becomes weaker - which slows down the ICD process again. At some point in h_{E} the lower Coulomb repulsion ultimately wins over the enhanced polarization, thus leading to the explicit maximum.

Interdependence of ICD on geometrical parameter variations

To study the interdependence of the ICD rate on the various geometric parameters at the same time, we will not only consider variations in h_{E}, but simultaneously probe a limited number of different values of the other parameters h_{A} and R. We start the discussion by performing scans of the ICD rates for h_{E} at different h_{A} but still for a fixed inter-QD distance of $R = 86.62$ nm (cf. Fig. 10). Note that five of the curves presented in figure 10 were calculated for the range of $h_{\mathrm{E}} = [14.73, \ldots, 19.34]$ nm, while four screens were performed in shorter ranges of about one nanometer around spline-interpolated estimate positions of the other maxima. All details on the rate-maximizing geometries at the maxima are collected in table 3.

In accord with the monotonous increase of Γ_{ICD} when increasing only h_{A}, one can see that the curves as a whole are in almost all points higher for larger values of h_{A}. This behaviour was discussed earlier in the short summary and is attributed to both lower virtual photon energies E_{vph} (cf. eq. (1)) as well as an increasing Coulomb repulsion $\tilde{E}_{\mathrm{Cou}}$ - both of which can also be confirmed in table 3, where we list the properties of the geometries leading to the maxima. A new observation that could only be made by changing the AQD height at the same time as the EQD height is that the specific EQD height which leads to the maximum in Γ_{ICD} (denoted h_{E}^{max}) does not remain constant for different h_{A}. Still, one can see that the h_{E}^{max} are following a rather smooth behaviour even when varying h_{A}. Considering that the maximum in Γ_{ICD} is related to the polarization of the E0 electron, it is sensible that changes of the A1 electron density will also have an influence on the position of h_{E}^{max}.

To understand the underlying interdependence of the ICD rate Γ_{ICD} with respect to both h_{A} and h_{E}, we need to combine these results with the interpretations made in the previous section. As changes in the AQD height have a higher impact on the Coulomb repulsion than that of the EQD height, we shall divide the discussion on three different regions of AQD

heights.

For low AQD heights, the ICD rates Γ_{ICD} are overall smaller due to the lower Coulomb interaction and the strong polarization towards the AQD (cf. Tab. 3). When changing the EQD height, no large changes are expected for the ICD rate, polarization, and Coulomb repulsion, because the interaction between the two QDs is weaker anyway. To obtain an optimal ICD rate in such a scenario, the rate-maximizing EQD heights h_{A}^{max} need to be larger than in case of small effective distances R_{eff}, as only then a favourable polarization can be achieved.

For intermediate AQD heights, the overall Coulomb interaction between the QDs becomes stronger, which also renders changes in the geometry of the EQD more important for the ICD rate. In this region, the rate-maximizing h_{E}^{max} is found at smaller heights than in the weak interaction region, because a more sensitive balance between polarization and Coulomb repulsion is needed as both terms become equally important for the process.

Finally, for even higher values of h_{A}, h_{E}^{max} becomes larger again. At this point, the potential wells may start overlapping, as the barrier separating the wells does not reach a value of zero between the QDs any more. Hence, from this point on tunneling processes become more and more available and consequently the asymptotic approximation does not hold any longer. Therefore, the decay displayed by such geometries is not caused by pure ICD, which is by definition an intermolecular rather than intramolecular process.

Next, we include the last missing parameter R in the discussion of the h_{E}^{max} values as well. To do this, we plot the respective rate-maximizing EQD heights h_{E}^{max} for a specific set of R and h_{A} in figure 11. One notices that in general a higher inter-QD distance R leads to higher values of h_{E}^{max}. This can be directly related to the fact that the greater distance lowers both the Coulomb repulsion as well as the polarization. Consequently, the EQDs must become larger to experience the same polarization as for smaller distances.

When comparing the plots of h_{E}^{max} for the different inter-QD distances R (cf. Fig. 11), all curves show an increase of the rate-maximizing EQD height at lower values of h_{A} and all of them decrease again after a maximum. Eventually, the curves for $R = 86.62$ nm and $R = 97.52$ nm increase again for even higher h_{A} which is, however, due to the overlap of the potential wells - and therefore not considered for the discussion of ICD processes (indicated

by hollow markers and dashed lines). It is informative to note, that the minima in h_{E}^{max} for $R = 86.62$ nm and $R = 97.52$ nm are almost separated by exactly the difference in their respective values of R.

Finally, the actual interdependence of Γ_{ICD} on the geometric parameters shall be discussed for all the ICD rate-maximized EQD geometries. To capture all geometric information at once, we first collect the data of h_{E}^{max} and h_{A} in a composite variable, which we call the rate-maximizing height ratio χ defined as

$$\chi(h_{\mathrm{A}}; R) = \frac{h_{\mathrm{A}}}{h_{\mathrm{E}}^{max}}. \tag{13}$$

As can be seen in figure 12, the composite variable χ is a non-linear function of h_{A} that is almost uniquely defined and almost strictly monotonously increasing with h_{A}, except for the first data point of $R = 108.36$ nm. It is informative to note, that in all rate-maximized PQD geometries, the AQD remains at least 1.6 times higher than the EQD. The region, where the asymptotic approximation breaks down can be directly related to when the curvature of χ becomes negative for higher h_{A}.

When then plotting the rate-maximized ICD rates against the respective values of χ (cf. figure 13), we may extract the whole interdependence of Γ_{ICD} on the geometric parameters. Firstly, we notice that lower inter-QD distances R in general produce a higher ICD rate for all values of χ. Secondly, a higher χ value also results in a higher value of Γ_{ICD}, which simultaneously means that high values of h_{A} lead to a faster decay, as χ monotonously increases with h_{A}. Additionally, whether increasing or lowering h_{E} from the optimized value, one always obtains worse rates.

Finally, one can see that for low values of χ the curves for different inter-QD distances R seem to follow the same behaviour until they eventually separate from each other. This result presents two major implications for the ICD process in charged PQD systems. Firstly, we can see that there exists a quantum physical upper bound to Γ_{ICD} for a given rate-maximized height ratio, that may or may not be achieved by the PQD geometry depending on the chosen inter-QD distance R. Secondly, as soon as the upper bound cannot be achieved any more, the curve for a given R branches off the general behaviour. The lower the inter-QD distance was chosen, the later the deviation occurs. The branching off the boundary behaviour is,

however, not caused by the breakdown of the asymptotic approximation, as this occurs only for much higher values of χ.

In the end, the rate-maximized geometry for ICD is found for high AQD heights h_A and small inter-QD distances R. The required EQD height h_E for the highest rates is determined by an optimal balance of the decreasing Coulomb repulsion $\tilde{E}_\mathrm{Cou}$ and the growing polarization $\langle q \rangle$ of the E0 electron.

CONCLUSIONS

In this work we present triplet-spin electron dynamics calculations using the antisymmetrized multiconfiguration time-dependent Hartree (MCTDH) method in a pseudo one-dimensional model system that reflects a doubly-charged, paired quantum dot (PQD). Performing a scan of over 1000 geometries, we study the dependence of the intermolecular Coulombic decay (ICD) process on the overall PQD geometry and especially focus on the interdependence of the ICD rate on changes in various parameters at the same time.

As we had not covered changes in the height of the electron emitting quantum dot (EQD) with our previous studies yet, we started by scanning this parameter individually. We found that there exists a maximum in the ICD rate with respect to the EQD height, which we ascribe to competing effects in the polarization and Coulomb repulsion.

We then discovered that changing other geometric parameters like the photon absorber QD (AQD) height or the inter-QD distance changes both the value of the maximum in the ICD rate as well as its position in terms of the EQD height. While the general trends for the ICD rate were already known for these two parameters, the changes in the position of the maximum point out the non-trivial nature and interdependence of the ICD process, such that one may not optimize one or the other QD separately. This result also shows that the asymptotic approximation may not be sufficient to fully describe the ICD process in quantum dots.

Finally, we propose an ICD rate-maximized geometry for a charged PQD system with a decay time of 102.39 ps in real units of GaAs. In this optimized set-up the cylindrical QDs are vertically-aligned, the EQD has a height of 16.33 nm, and the AQD a height of 46.59

nm. The inter-QD distance of this set-up equals 86.68 nm and the radii of the cylinders were 14.42 nm for both QDs.

ACKNOWLEDGMENTS

We thank the Volkswagen foundation for financial support (Freigeist Fellowship No. 89525). Furthermore, we acknowledge fruitful discussions with K. Gokhberg about polarization effects.

References

1. Cederbaum, L. S., Zobeley, J., Tarantelli, F., Phys. Rev. Lett., **1997**, 79, 4778.
2. Auger, P., Comptes Rendus, **1925**, 180, 65.
3. Cederbaum, L. S., Zobeley, J., Tarantelli, J. Chem. Phys. A, **1999**, 103, 11145.
4. Marburger, S., Kugeler, O., Hergenhahn, U., Möller, T., Phys. Rev. Lett., **2003**, 90, 203401.
5. Aziz, E. F., Ottosson, N., Faubel, M., Hertel, I. V., Winter, B., Nature, **2008**, 455, 89.
6. Schöffler, M. S., Kim, H.-K., Sturm, F. P., Cole, K., Neumann, N., Vredenborg, A., Williams, J., Bocharova, I., Guillemin, R., Simon, M., Belkacem, A., Landers, A. L., Weber, Th., Schmidt-Böcking, H., Dörner, R., Jahnke, T., Nature, **2014**, 505, 664.
7. Müller, I. B., Cederbaum, L. S., J. Chem. Phys., **2006**, 125, 204305.
8. Kryzhevoi, N. V., Cederbaum, L. S., J. Phys. Chem. B, **2011**, 115, 5441.
9. Jabbari, G., Klaiman, S., Chiang, Y.-C., Trinter, F., Jahnke, T., Gokhberg, K., J. Chem. Phys., **2014**, 140, 224305.
10. Averbukh, V., Müller, I. B., Cederbaum, L. S., Phys. Rev. Lett., **2004**, 93, 263002.
11. Mucke, M., Braune, M., Barth, S., Förstel, M., Lischke, T., Ulrich, V., Arion, T., Becker, U., Bradshaw, A., Hergenhahn, U., Nature Physics, **2010**, 6, 143.
12. Norris, D. J., Efros, Al. L., Rosen, M., Bawendi, M. G., Phys. Rev. B, **1996**, 53, 16347.
13. Schooss, D., Mews, A., Eychmüller, A., Weller, H., Phys. Rev. B, **1994**, 49, 17072.
14. Beck, M. H., Jäckle, A., Worth, G. A., Meyer, H.-D., Phys. Rep., **2000**, 324, 1.
15. Multidimensional Quantum Dynamics; Meyer, H.-D.; Gatti, F.; Worth, G. A., Eds.; Wiley-VCH, **2009**.
16. Ashoori, R. C., Nature, **1996**, 379, 413.

17. Bande, A., Gokhberg, K., Cederbaum, L. S., J. Chem. Phys., **2011**, 135, 144112.

18. Bande, A., J. Chem. Phys., **2013**, 138, 214104.

19. Haller, A., Chiang, Y.-C., Menger, M., Aziz, E. F., Bande, A., Chem. Phys., **2017**, 482, 135.

20. Dolbundalchok, P., Peláez, D., Aziz, E. F., Bande, A., J. Comput. Chem., **2016**, 37, 2249.

21. Electronic archive: New Semiconductor Materials. Characteristics and Properties. Basic Parameters of Gallium Arsenide. Available at: http://www.ioffe.ru/SVA/NSM/Semicond/GaAs/basic.html (accessed November 7, **2016**).

22. Bednarek, S., Szafran, B., Chwiej, T., Adamowski, J., Phys. Rev. B, **2003**, 68, 045328.

23. Bande, A., Pont, F. M., Dolbundalchok, P., Gokhberg, K., Cederbaum, L. S., EPJ Web. Conf., **2013**, 41, 04031.

24. Muga, J. G., Palao, J. P., Navarro, B., Egusquiza, I. L., Phys. Rep., **2004**, 395, 357.

25. Stumpf, V., Brunken, C., Gokhberg, K., J. Chem. Phys., **2016**, 145, 104306.

Figure 1: Binding potential curves of the PQD (eq. (2)) in z-direction for the shortest (top) and longest (bottom) inter-QD distances R in consideration. The solid lines in both panels reflect the uppermost height values h_{A} and h_{E} while the dashed lines give the respective other extreme. The numbers may be taken from Tab. (1).

Figure 2: One-electron densities of the A0E0 (bottom), the first continuum-like A0C (middle), and the A1E0 resonance eigenstates (top) in energetic ordering. Black circles indicate the QD positions. The one-electron densities of the A0E0 and A1E0 states are strictly localized around the QDs, while the A0C state has electron density to the far right, reflecting its unbound character.

Figure 3: Eigenenergies of electronic states for varying EQD heights h_{E}. Dashed lines represent every second of the continuum-like states, while solid lines show the states A0E0 and the first continuum-like eigenstate A0C. All eigenenergies were shifted such that the first A0C state represents the continuum threshold with zero energy. The dots mark the resonance-like state A1E0.

Figure 4: The zoom into the eigenenergies close to the resonance-like state shows a non-degenerate state-to-state transition at h_{E}= 19.0 nm and a near-degenerate avoided crossing at h_{E}= 19.6 nm. The solid line with point-markers represent the A1E0 state, while dashed and dash-dotted lines give the continuum-like states. Note, how the j^{th} state turns into the $(j-1)^{\mathrm{th}}$ state and so on.

Figure 5: (from top to bottom) Densities of the near-degenerate $(j-1)^{\mathrm{th}}$ and the $(j-2)^{\mathrm{th}}$ states at the avoided crossing of 0.04 meV at $h_{\mathrm{E}} = 19.6nm$ (cf. Fig. 4). Black circles indicate the position of the QDs.

Figure 6: Expectation value of the Coulomb energy for different h_{E} as approximated by eq. (11) with a local minimum at $h_{\mathrm{E}} = 18.91$ nm.

Figure 7: Expectation values of the real part of the total dipole moment as a function of h_{E} as approximated by eq. (12).

Figure 8: Logarithmic autocorrelation functions for different PQD geometries (cf. Tab. 2). The geometries are derived from a default system D, where the h_{E} parameter is changed to a set of different values to show the general trends. The minus and plus signs indicate whether the height was increased or decreased, while the number represents the magnitude of the change.

Figure 9: ICD rates Γ_{ICD} for the screen of the EQD heights h_{E} at fixed $R = 86.62$ nm and $h_{\mathrm{A}} = 36.08$ nm

Figure 10: ICD rates Γ_{ICD} as functions of EQD heights h_{E} for different AQD heights h_{A} given in nanometers beside the curves. Five curves have been calculated for the full h_{E} range from 14.73 to 19.34 nm, whereas the shorter curves were calculated on a small range around the spline interpolated estimations of the location of their maxima. The dashed line is connecting the maxima of the curves.

Figure 11: EQD heights h_{E}^{max} for which a maximum Γ_{ICD} is found as a function of the AQD height and inter-QD distance R. Dashed lines as well as hollow markers indicate that these results were obtained for non-separate QD wells.

Figure 12: Rate-maximizing height ratios χ (eq. (13)) as function of AQD heights at the three different QD inter-QD distances R. The ratios are calculated for the geometries with maximum ICD rates. Dashed lines, as well as hollow markers indicate that these results were obtained for non-separate QD wells.

Figure 13: ICD rates as a function of the rate-maximized height ratios χ for different inter-QD distances R. Dashed lines, as well as hollow markers indicate that these results were obtained for non-separate QD wells.

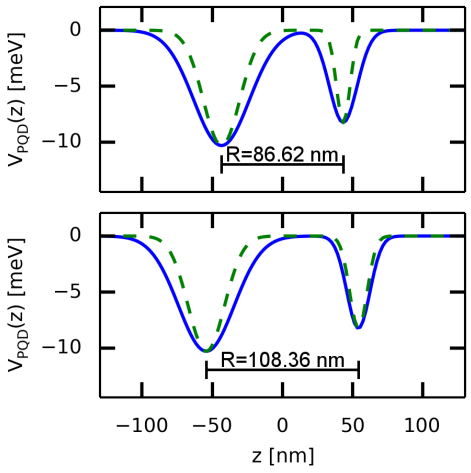

Frontier cases of the PQD model potential
Fabian Weber
J. Comput. Chem.

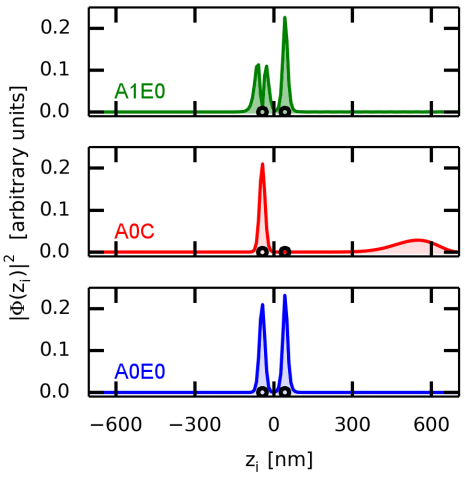

One-electron densities of the three significant states
Fabian Weber
J. Comput. Chem.

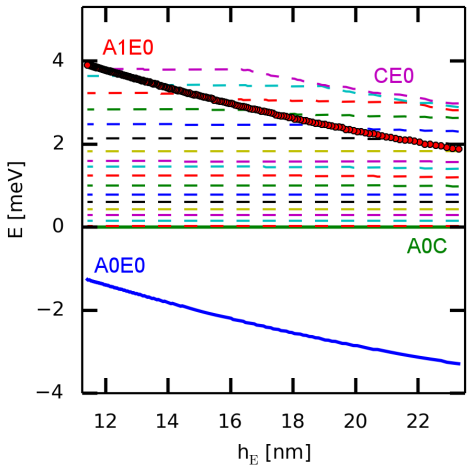

Eigenenergies of the bound, resonant and continuum-like states
Fabian Weber
J. Comput. Chem.

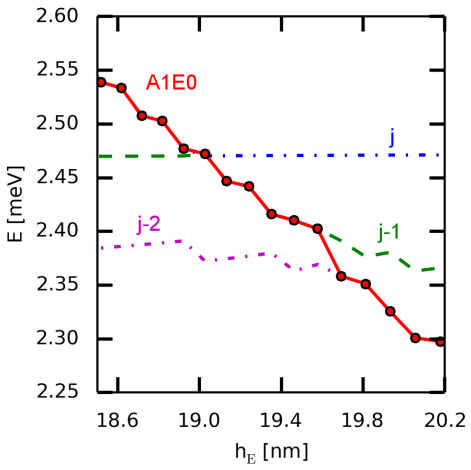

Zoom into the eigenenergies - especially into an avoided crossing
Fabian Weber
J. Comput. Chem.

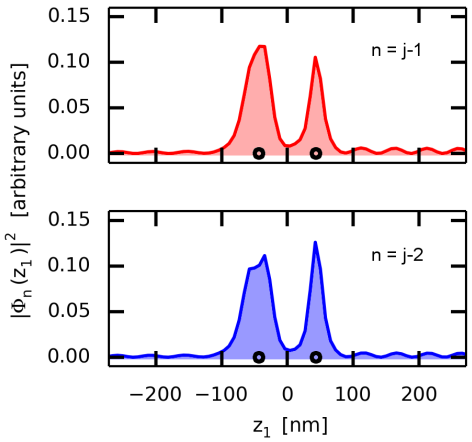

Degenerate one-electron densities at an avoided crossing
Fabian Weber
J. Comput. Chem.

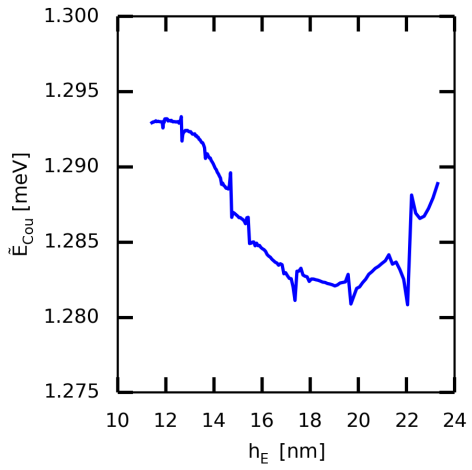

Modified expectation value of the Coulomb repulsion
Fabian Weber
J. Comput. Chem.

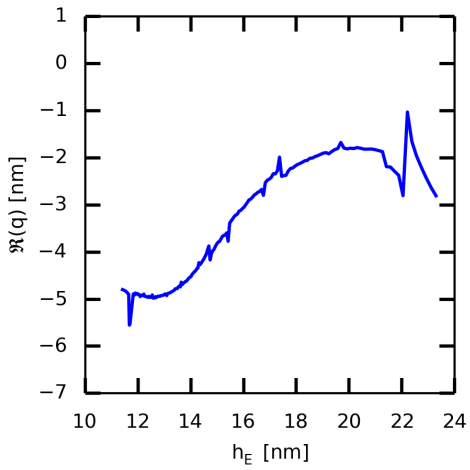

Modified expectation value of the position operator
Fabian Weber
J. Comput. Chem.

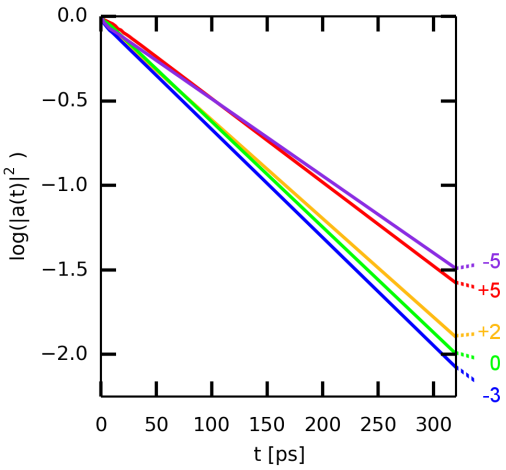

Logarithmic Autocorrelation Functions for frontier geometries
Fabian Weber
J. Comput. Chem.

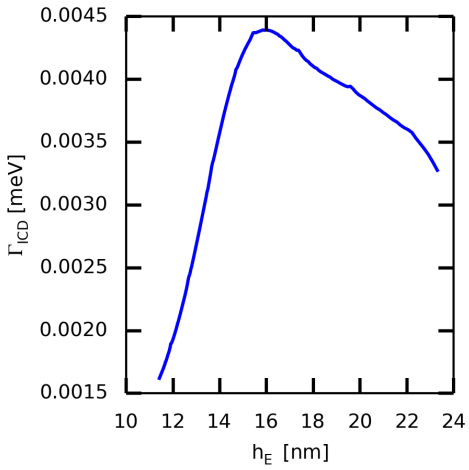

Large scan of the ICD rate woth respect to the EQD height
Fabian Weber
J. Comput. Chem.

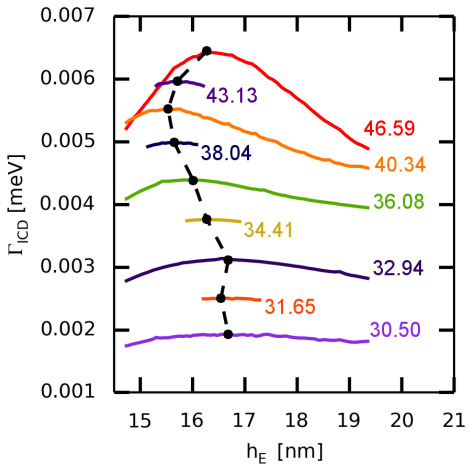

Scans of Gamma for different EQD and AQD heights
Fabian Weber
J. Comput. Chem.

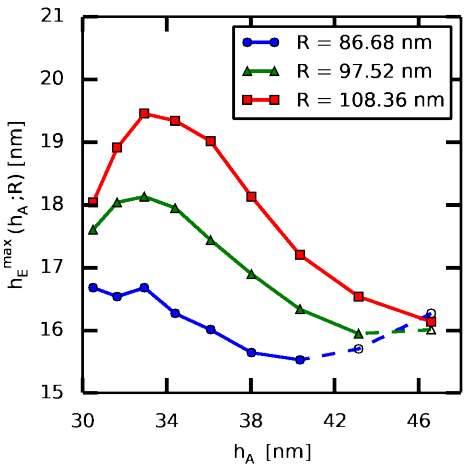

ICD rate-maximizing EQD heights for different inter-QD distances and AQD heights
Fabian Weber
J. Comput. Chem.

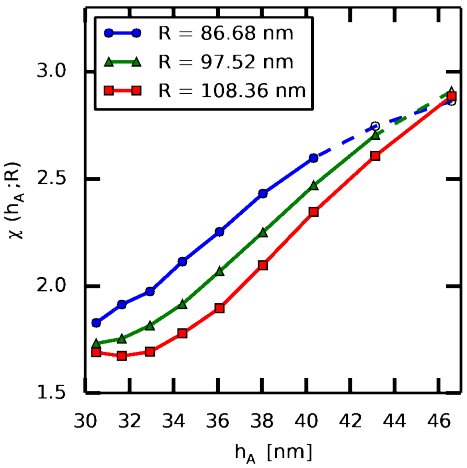

Rate-maximizing height ratios of EQD and AQD heigts for different AQD heights and inter-QD distances
Fabian Weber
J. Comput. Chem.

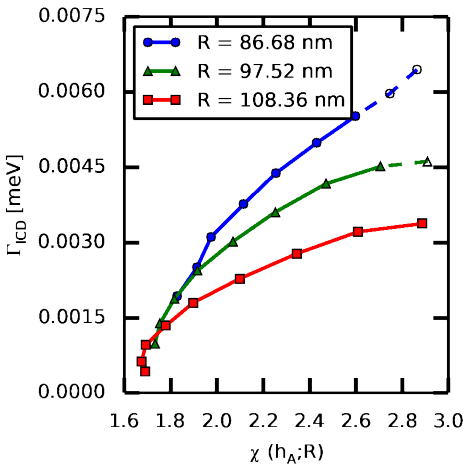

ICD rates for different rate-maximizing height ratios and inter-QD distances
Fabian Weber
J. Comput. Chem.

Parameter	**Range** [a.u.]	**Resolution** [a.u.]	**Range** [nm in GaAs]
R	[8.00, ..., 10.00]	1.00	R=[86.68, ..., 108.36]
b_{A}, h_{A}	[0.15, ..., 0.35]	0.05	h_{A}=[46.59, ..., 30.50]
b_{E}, h_{E}	[0.60, ..., 2.50]	0.01	h_{E}=[23.29, ..., 11.41]

Table 1: Total parameter ranges for the scan of the geometries. Note that the EMA conversion from $b_{\mathrm{A/E}}$ to real units of GaAs includes transforming the parameters into the respective heights.

Label	$\mathbf{h_E}$ **[nm]**	τ_{ICD} [ps]	Γ_{ICD} [10^{-3}/meV]
+5	23.29	202.01	3.2583
+2	20.17	171.24	3.8439
0	18.04	160.54	4.0964
−3	14.98	156.36	4.2096
−5	13.34	219.34	3.0009

Table 2: Geometric parameters and decay times τ_{ICD} for probing changes in the EQD height parameter. The geometries are derived from a default case 0 ($h_{\mathrm{A}} = 36.08$ nm, $h_{\mathrm{E}} = 18.04$ nm and $R = 86.62$ nm) and carry labels corresponding to the approximate changes in h_{E} in nanometers with respect to the default case. The corresponding autocorrelation plots are collected in (cf. Fig 8).

$\mathbf{h}_\mathrm{A}$ [**nm**]	$\mathbf{h}_\mathrm{E}{}^{max}$ [**nm**]	E_vph [meV]	$\tilde{E}_\mathrm{Cou}$ [meV]	$\langle q \rangle$ [nm]	τ_ICD [ps]	Γ_ICD [10^{-3}/meV]
46.59	16.26	4.425	1.299	-3.070	102.4	6.450
43.13	15.70	4.669	1.293	-2.230	110.2	5.971
40.34	15.53	4.842	1.292	-2.219	119.1	5.522
38.04	15.64	5.031	1.287	-2.174	131.9	4.989
36.08	16.01	5.147	1.285	-3.131	149.8	4.384
34.41	16.27	5.291	1.277	-3.771	174.7	3.766
32.94	16.68	5.392	1.271	-5.358	209.7	3.116
31.65	16.54	5.485	1.258	-7.089	262.7	2.506
30.50	16.68	5.540	1.241	-9.706	341.0	1.933

Table 3: Properties of rate-maximizing PQD geometries for $R = 86.62$ nm